Optical and thermochromic properties of yttrium iron garnet paint

A Rostamnejadi[*], M M Madahi Harandi, and M Jazirehpour

Faulty of Electromagnetics, Malek Ashtar University of Technology, Iran.

E-mail: rostamnejadi@mut-es.ac.ir

Abstract

In this study, we have investigated the optical and high-temperature thermochromic properties of yttrium iron garnet powder and paint. The powders were produced using the solid-state reaction technique, and the thermochromic paint was sprayed over an Al alloy substrate. X-ray diffraction patterns, optical and field emission scanning electron microscopes, and UV-Vis and FTIR spectrophotometers were used to assess the structural, surface morphology and optical characteristics of the materials. The thermochromic characteristics of the samples were investigated by extracting the chromatic coordinates L*b*a* from digital pictures taken at temperatures ranging from 25 to 210 °C. The results reveal that when the temperature rises, the color of the paint changes from dark green to dark brown. The charge transfer between oxygen and iron ions, as well as the electron transition across the orbitals of the d layer, could be responsible for the observed reversible color change. The paint has strong thermal stability up to 350 °C which is suitable for high-temperature thermochromic applications.

Keywords: thermochromic, high temperature paint, yttrium iron garnet, powder.

1. Introduction

Intelligent materials exhibit reversible physical activity in response to external inputs [1]. Chromogenic materials change their color in response to external stimuli such as temperature, voltage and pressure [1, 2]. Thermochromic materials are temperature sensitive over a wide operating temperature range. Thermochromic coatings and paints have many civil and military potential applications, including energy consumption and sunlight irradiation control in buildings and windows, thermometers and temperature sensors, laser marks, thermal warning signals, smart textiles and intelligent temperature control coatings, spacecraft thermal management, visible-infrared smart stealth and adaptive camouflage technology [2-16].

In recent decades, several thermochromic materials, including polymers, organic and inorganic materials, have been explored [2, 3, 5, 7, 17-20]. Because of their limited thermal stability and detrimental effects on organisms, organic thermochromic chemicals are utilized at temperatures lower than 125 °C. Due to their great durability and strong thermal and chemical stabilities, inorganic substances are viewed as viable alternatives for higher temperatures. Metal oxides and salts are two groups of high temperature inorganic thermochromic materials. Salt compounds such as AgI, Ag_2HgI_4, Cu_2HgI_4 exhibit thermochromic characteristics in both the solid and soluble states, and their working temperature is less than 300 °C. The thermochromic characteristics of oxides are often reversible in visible or infrared areas across a large temperature range from room temperature to about 800 °C. Metal oxides such as TiO_2, ZnO, WO_3 and VO_2 exhibit thermochromic effect in the visible area. Some oxides including V_2O_5, nanoparticles of VO_2, Co-doped zinc oxide, and metamaterials exhibit thermochromic characteristics in the near-infrared region [4, 9, 11, 14, 21-28].

Garnets are a well-known kind of magnetic oxides that are utilized in radars, telecommunications, RF measuring systems, and microwave devices such as circulators, isolators, phase shifters, and tunable filters. Because of its importance in magneto-optical and microwave devices, Yttrium iron garnets (YIG) is an intriguing ferrimagnetic oxide [29-35]. Several groups have explored the optical properties of garnet single crystals, thin films, and powders [22, 23, 33, 34, 36-39]. The presence of Fe^{3+} ions in iron oxides generally results in red coloration in Fe_3O_4, Fe_2O_3, $ZnFe_2O_4$ and $MgFe_2O_4$, however it results in a comparatively green coloration in YIG. Several publications on the thermochromic characteristics of garnets have recently been published. Reversible and

continuous thermochromism has been seen in the visible range with high durability and thermal stability from room temperature to beyond 500 °C [22, 29-34, 36, 40]. From ambient temperature to 220 °C, the color shift from greenish to brownish was noticed in polycrystalline YIG [30]. Only chromium ions have been found to efficiently affect the color of the parent material among many dopants such as Al^{3+}, Ga^{3+}, Mn^{3+}, and Cr^{3+} [30]. Liu et al. investigate the influence of grain size on the optical and thermochromic characteristics of $Sm_3Fe_5O_{12}$ garnet from room temperature to 240 °C [23]. The color shift from yellow-green to reddish brown is connected to ongoing structural evolution and Fe^{3+}-O bond length stretching, according to temperature-dependent XRD and UV-Vis spectra investigations. Liu et al. recently reported reversible multicolor thermochromic characteristics in $Cr^{3+}/Mn^{3+}/Fe^{3+}/Co^{3+}$-doped $Er_3Ga_5O_{12}$ from ambient temperature to 460 °C [40]. While there are some high-temperature thermochromic materials such as garnets [22, 30, 38, 40], yttrium-substituted bismuth oxides [41], and Cr-doped Al_2O_3 [21, 42], but high-temperature thermochromic coatings and paints have not been thoroughly investigated for fundamental research and prospective applications. In this study, we have investigated the thermochromic characteristics of YIG paint in the temperature range of 25 to 210 °C for the first time.

2. Experimental section

2.1. Preparation of YIG powders and paint

The traditional solid state reaction approach was used to create Y_3Fe5O_{12} powders from Y_2O_3, Fe_2O_3 oxides in a 3:5 molar ratio. For 120 minutes, the raw materials were processed in a fast mill with a ball-to-powder weight ratio of 8:1. An electric oven was used to dry the final mixture at 90 °C. After grinding, the dried powders were put in an alumina crucible and heated at 1200 °C for 4 hours (S-1200) and 1400 °C for 6 hours (S-1400) at a temperature rate of 4.8 °C/min in an electric furnace. After calcination, the powders were processed for 6 hours in a fast mill to uniform the particles. A silicone-based resin, Ren68, was used as a matrix to create the thermochromic paint. To begin, 3 g of Ren68 was dissolved in 5 g of acetone and agitated until a clear solution was obtained. The solution was then tinted with 5 g of yttrium iron garnet powder (S-1400) and heated at 50 °C for 10 minutes. The existence of pores and roughness on the surface of the paint can play key roles in causing optical contrast error. To avoid this error, the pigment was carefully ground and passed through a strainer before preparing the paint. To promote paint adherence, the aluminum alloy substrate was scraped with a copper brush before being heated at 70 °C in an electric oven. Following the heating of the substrate, the paint was coated using a spray gun and then heated at 250 °C to eliminate the volatiles.

2.2. characterization methods

To confirm the crystalline phase formation of YIG and check the existence of secondary phases, the X-ray diffraction (XRD) spectra of the powder samples have characterized using a Philips X'Pert PRO X-ray diffractometer by Cu-Kα X-ray source (λ=1.5406 Å). The Rietveld analysis of the XRD spectra have carried out by Maud-2019 software. The samples' morphology and surface quality were examined using an optical microscope and a field emission scanning electron microscope (FE-SEM; FEI Quanta 450 FEG). The reflectance spectra of the samples were measured using a UV-Vis spectrometer (JASCO, V-670) and a FTIR spectrometer in the wavelength range of 200 nm- 24 μm. Surface images were obtained using a Nikon P900 digital camera with 1200×1600 pixel resolution to investigate the thermochromic properties of the samples. The camera was placed 20 cm away and at a 30-degree angle to the surface of the samples. The surface of the samples was then photographed at temperatures of 25, 50, 100, 150, and 210 °C using an electric heater with temperature accuracy about 5 °C. A white light bulb was used to give ambient light while also preventing shadows forming. The CIE-L*a*b* model was used to quantitatively examine the color change of the samples.

3. Results and discussion

3.1. Structural analysis and surface morphology

Figure 1 depicts the X-ray diffraction patterns of the powder samples after Rietveld refining. According to Fig. 1, there is a secondary phase of $YFeO_3$ in the S-1200 sample at around 17 weight percent. Rietveld examination of the structural results reveals that $Y_3Fe_5O_{12}$ has a cubic structure with a $Ia\bar{3}d$ space group and $YFeO_3$ has an orthorhombic structure with a Pnma space group. The secondary phase dissolved when the calcination temperature increased from 1200 °C to 1400 °C, and the lattice constant of $Y_3Fe_5O_{12}$ increased slightly from 12.375 Å to 12.378 Å.

In practical applications, thermochromic materials with thermal, chemical, and mechanical stabilities must be coated on desirable surfaces. The thermochromic characteristics of the YIG paint created from S-1400 powder will be investigated in the next section. The paint is made from a high-temperature stable silicon resin that is thermally stable up to 600 °C. Figure 2 depicts a digital picture of the paint at room temperature as well as an optical microscope image. The optical microscope picture indicates that the surface of the paint is almost smooth and has a roughness of around 20 micrometers. Figure 2(c) shows a FE-SEM micrograph of the thermochromic paint after heating at 600 °C. When heated, the paint demonstrated great adhesion and thermal durability up to 350 °C. However, at higher temperatures, despite the excellent adhesion, there are many cracks and voids on the paint's surface due to resin shrinkage. As a result, the paint's mechanical and thermal stabilities for high-temperature applications must be improved..
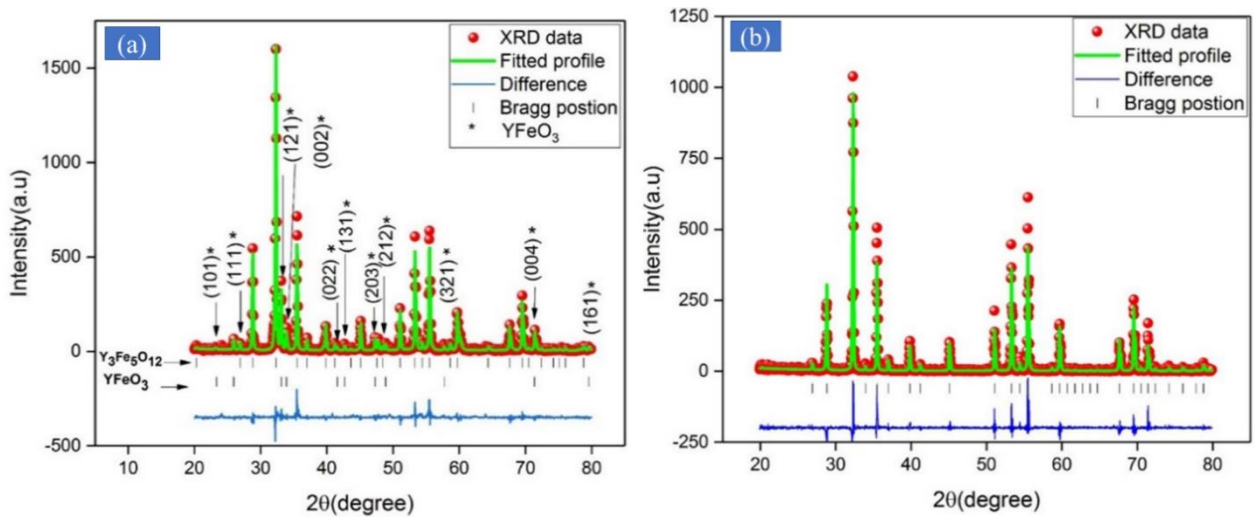
Figure 1. XRD spectra of the garnet powder samples with their Rietveld analyses: (a) S-1200 and (b) S-1400.
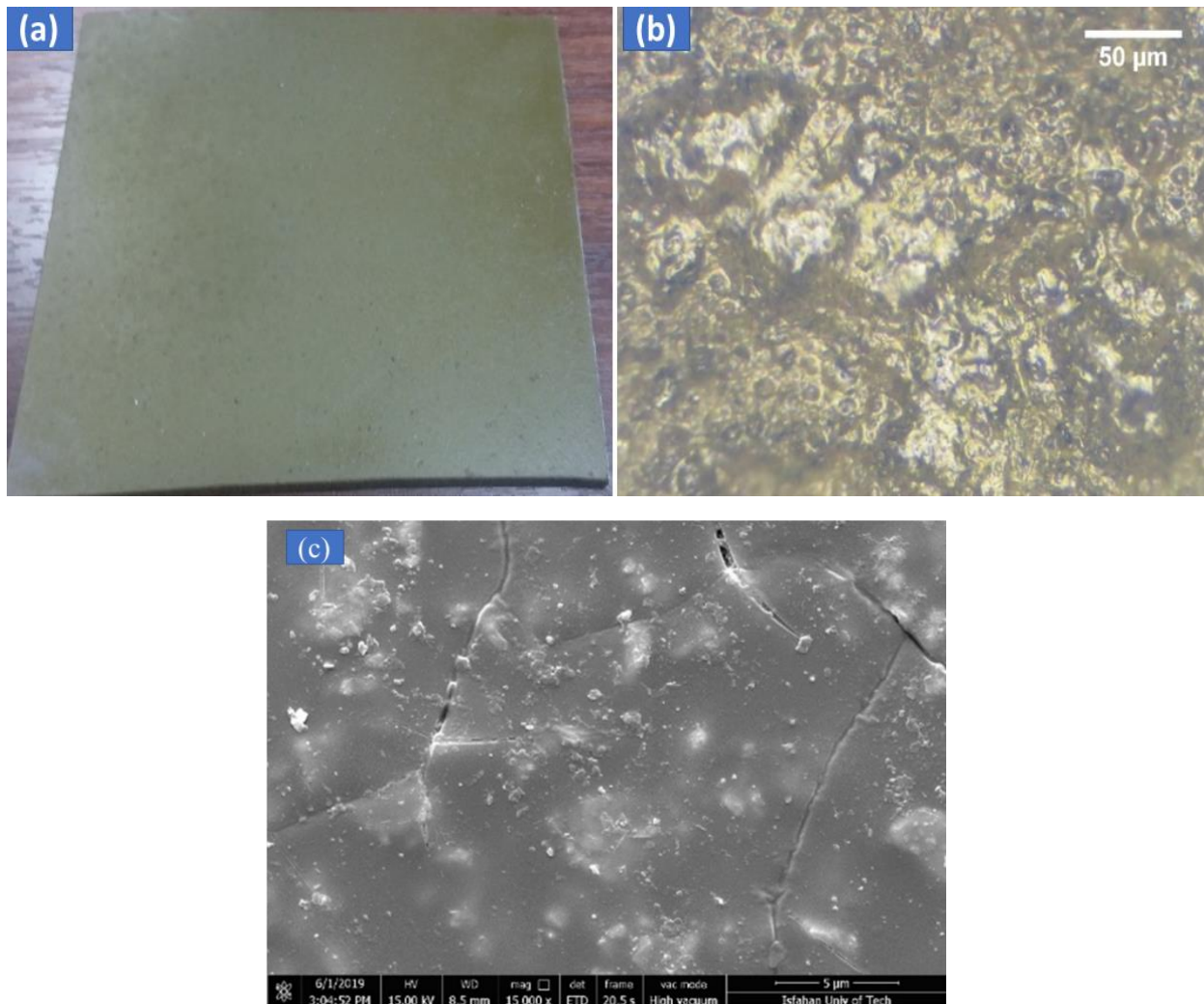

Figure 2. (a) A digital photograph and (b) an optical micrograph of the surface of YIG paint at room temperature. and (c) FE-SEM micrograph of the paint after heating at 600 °C.

3.2. Optical and thermochromic properties

S-1400 sample was dissolved in ethylene glycol and then coated on standard glass using a spin coating machine to analyze the transmission spectra. Figure 3 depicts the transmission spectra of the coated sample measured at room temperature in the wavelength range of 200 to 2000 nm. The absorption spectrum is determined using the measured transmission spectrum and the following equation [43].

$$\alpha = (1/d) \, log \, (1/T), \tag{1}$$

In this equation, α is the absorption coefficient, T is the transmittance, and d is the layer thickness, which is unknown in this case and might be regarded an optional parameter. According to figure 3(b), the sample's absorption spectrum is minimal up to an energy of 3.8 eV ($\lambda \sim 326$ nm), but beyond that, the dominating absorption emerges.

Figure 4 depicts the normal reflectance spectra of the YIG paint in the UV-Vis and infrared areas at room temperature. The optical properties of garnets are primarily originated from various mechanisms such as charge transfer between oxygen ions and iron ions, electron transition between iron ion d-levels and interband transition. The absorption peaks at wavelengths ranging from 400 to 600 nm are attributable to transitions caused by charge transfer between oxygen and iron ions [30, 42]. The d-d transitions, which cause the yttrium iron garnet green color shift, are responsible for the absorption peak in the wavelength range of 610 to 920. The energy of d-d transitions varies very slightly with temperature, whereas the absorption edge caused by charge transfer is closely proportional to temperature. The absorption peaks in the wavelength range of 2 to 25 µm in figure 4(b) could be attributed to the phonon absorption in the paint.

Figure 5 shows digital photos of YIG powder and paint at various temperatures. As shown in figure 5, the continuous and reversible color shift from green to brown and dark green to dark brown occurs for YIG powder and paint samples as the temperature rises from 25 to 210 °C. The increase in temperature had no influence on the color change of the paint at temperatures ranging from 210 to 350 °C. We employed the CIE-L*a*b* model to evaluate the color change of the samples.[44, 45] In this model, which is independent of displaying devices, the brightness, color shift from green to red and color change from blue to yellow are presented by L*, a*, and b* chromatic coordinates, respectively. For perfect black and flawless white, the L* value ranges from 0 to 100. The positive and negative values of a* represent the red and green colors, respectively. Similarly, positive and negative values of b* are represented by the yellow and blue colors, respectively. The chromatic coordinates of the YIG powder and paint in the temperature range of 25 to 210 °C are shown in figure 6. For YIG powder, as shown in figure 6(a), by increasing temperature L* and b* reduce from 44 to 31 and 36 to 30, respectively, whereas a* raises from -2 to 10. The chromatic coordinates of the YIG paint displayed the same behavior as the powder. L* and b* fall from 34 to 25 and 25 to 17, respectively,

whereas a* rises from -1 to 10. The thermochromic characteristics of YIG powder and paint observed in this work accord with the previously reported results for the garnet powder samples [22, 30, 40].

The origin of thermochromism in materials is a complex problem that could be related to temperature dependent various optical processes such as geometric changes in the ligands, changes in the number of molecules and coordination number, changes in the band gap energy, charge transfer between ions, and the presence of crystal structure defects. In inorganic substances, the electronic transition from the ground state to an excited state is connected to thermochromic characteristics in the visible area. The simultaneous existence of Fe^{3+} and Fe^{2+} ions in iron oxides can result in mixed valence states. The optical and thermochromic features of YIG garnet result from a combination of charge transfer between iron and oxygen ions, electron transitions in the 3d-layer of iron ions and interband transitions. The charge transfer energy between 2p levels of oxygen ions to the empty 3d levels of Fe^{3+} ions is approximately 2.57 eV. The energies of d-d transitions range from 1.35 to 2.04 eV, while the band gap energy of direct interband transitions is around 2.77 eV [22, 29, 30, 42]. Temperature increasing has a direct relationship with the continuous redshift of the absorption edge of the charge transfer and has a modest effect on the absorption energy of the d-d transition. A regular displacement happens when the ionic bond length increases with temperature, which is followed by a rise in the lattice constants. Increasing the lattice constants reduces the charge transfer between iron and oxygen ions, resulting a continuous and reversible color shift in yttrium iron garnet from green to brown.

4. Conclusion

For the first time, the thermochromic behavior of YIG paint at diverse temperatures ranging from 25 to 210 °C with thermal stability up to 350 °C was explored in this study. According to the results, the color of the YIG powder sample changes from green to brown, and the color of the paint changes from dark green to dark brown. For both YIG powder and paint, the chromatic coordinates L* and b* drop while the value of a* increases. The observed thermochroic effect in YIG powder and paint is related to the charge transfer between oxygen and iron ions, as well as the electron transition across the orbitals of the d layer. The thermal stability of the paint is suitable for high-temperature thermochromic applications

Declarations

Conflict of interest. The authors declare that they have no conflicts of interest in this research paper.
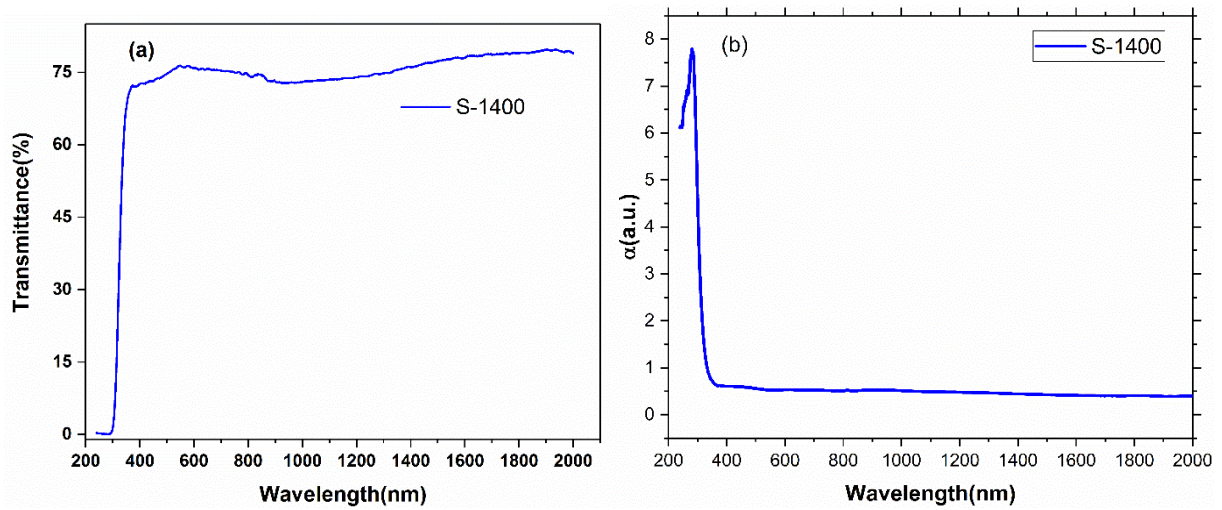
Figure. 3. (a) Transmission spectra and (b) absorption coefficient vs wavelength for (S-1400+ethylen glycol on glass).
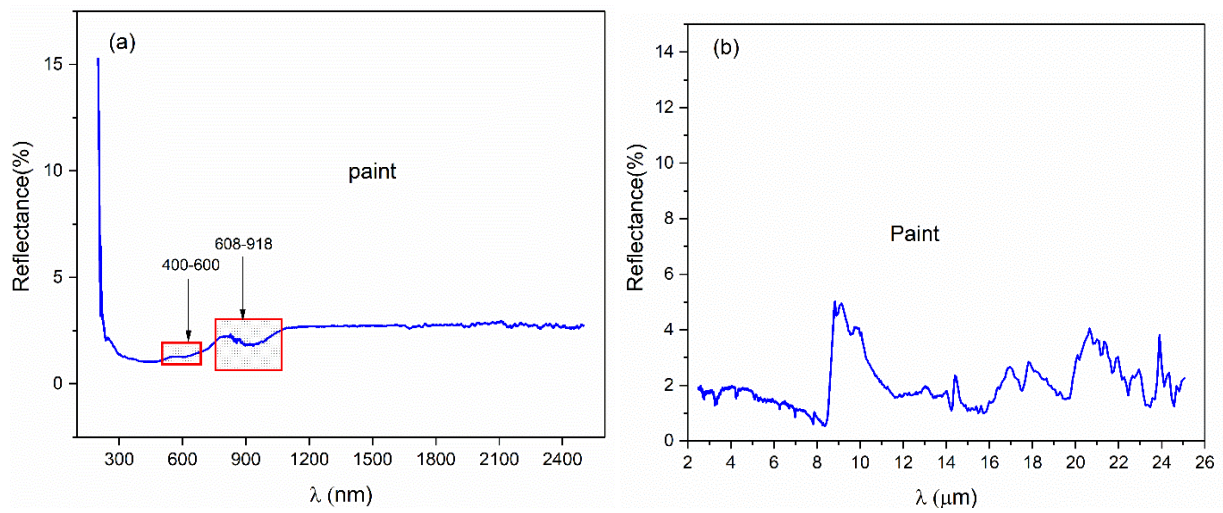
Figure 4. Reflection spectrum of the yttrium iron garnet paint in (a) UV-Vis-near IR and (b) mid IR regions.
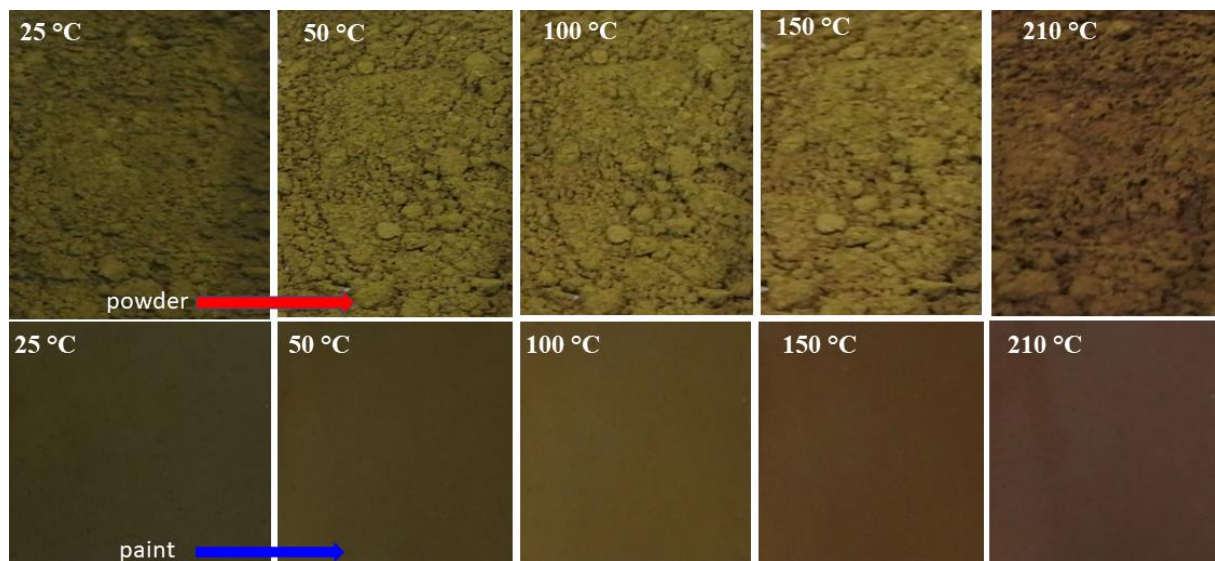
Figure 5. Digital photographs of the color change of YIG powder and paint at different temperature.
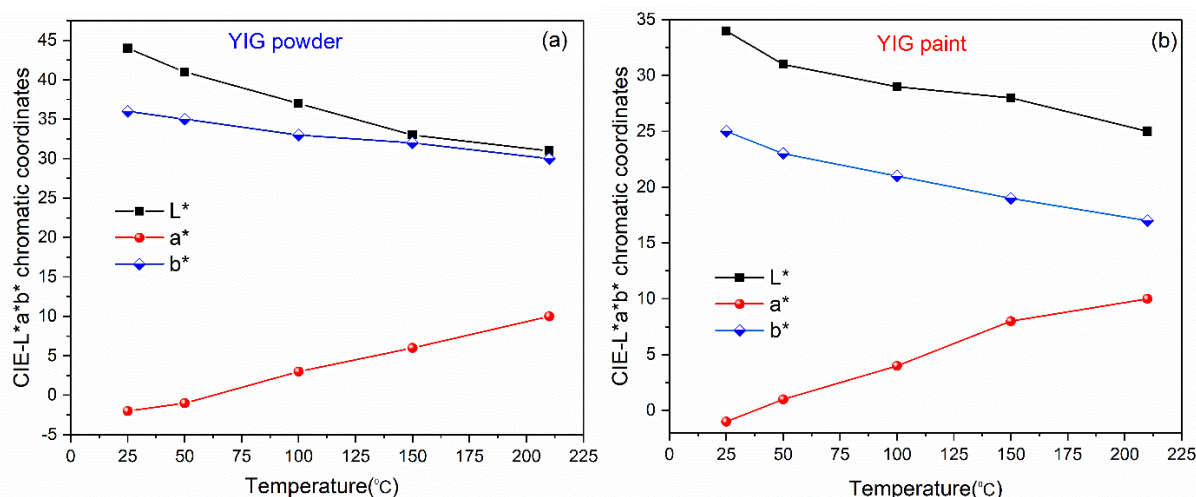
Figure 6. Variation of Chromatic coordinates of (a) YIG powder and (b) YIG paint versus temperature.

References

1. M Ferrara and M Bengisu, "*In Materials that Change Color*". Springer (2014).
2. C-G Granqvist, P Lansåker, N Mlyuka, G A Niklasson, and E Avendano, *Ener. Mater. Sol. Cells* **93** (2009) 2032.
3. X Zhao, X Hu, J Sun, Q You, H Xu, W Liu, G Sun, Y Nie, W Yao, and X Jiang, *J. Appl. Phys.* **128** (2020) 185107.
4. B Zhang, C Xu, G Xu, S Xiang, and Y Zhu, *Opt. Mater*. 86 (2018) 464.
5. Q Li, D Fan, and Y Xuan, *J. Alloys Compd*. **583** (2014) 516.
6. M Arulprakasajothi, B Susanth, K N Kumar, and A M M Reddy, *Mater. Today: Proc*. **47** (2021) 4666.
7. P S Aklujkar, and B Kandasubramanian, *J. Coat. Tech. Res*. (2020) 18.
8. J Kim and T Paik, *Nanomaterials* **11** (2021) 2674.
9. Y Zhu, G Xu, T Guo, H Hou, and S Tan, *J. Alloys Compd*. **720** (2017) 105.
10. S Zheng, Y Xu, Q Shen, and H Yang, *Sol. Energy* **112** (2015) 263.
11. S-Y Li, G A Niklasson, and C-G Granqvist, *J. Appl. Phys.* **108** (2010) 063525.
12. I P Parkin, and T D Manning, *J. Chem. Edu*. **83** (2006) 393.
13. M Štaffová, F Kučera, J Tocháček, P Dzik, F Ondreáš, and J Jančář, *J. Appl. Poly. Sci*. **138** (2021) 49724.
14. H Ji, D Liu, H Cheng, C Zhang, L Yang, and D Ren, *RSC Adv*. **7** (2017) 5189.
15. S Soudian, U Berardi, and N Laschuk, *Sol. Ener.* **205** (2020) 282.
16. T Karlessi, M Santamouris, K Apostolakis, A Synnefa, and I Livada, *Sol. Energy* **83** (2009) 538.
17. A Seeboth, D Lotzsch, R Ruhmann, and O Muehling, *Chem. Rev.* **114** (2014) 3037.
18. A Seeboth and D Lötzsch, "*Thermochromic and thermotropic materials*", CRC Press (2013).
19. Y Li, J Liu, D Wang, and Y Dang, *J. Electron. Mater* **46** (2017) 6466.
20. X-J Wang, Y-Y Liu, D-H Li, B-H Feng, Z-W He, and Z Qi, *Chinese Physics B* **22** (2013) 066803.
21. D K Nguyen, H Lee, and I-T Kim, Materials 10 (2017) 476.
22. H Liu, L Yuan, S Wang, H Fang, Y Zhang, C Hou, and S Feng, *J. Mater. Chem. C* 4 (2016) 10529.
23. H Liu, L Yuan, H Qi, Y Du, S Wang, and C Hou, *RSC Adv*. **7** (2017) 37765.
24. P He, W-X Huang, J-Z Yan, M-Y Zhi, J-H Cai, and R-R Luo, *Mater. Res. Bull*. 46 (2011) 966.
25. J Zhang, J Wang, C Yang, H Jia, X Cui, S Zhao, and Y Xu, *Sol. Ener. Mater. Sol. Cells* **162** (2017) 134.
26. I Mjejri, A Rougier, and M Gaudon, *Inorg. Chem.* **56** (2017) 1734.
27. X Liu, and W J Padilla, *Adv. Mater*. **28** (2016) 871.
28. M Zinzi, *Energy Build*. **114** (2016) 206.
29. E Mallmann, A Sombra, J Goes, and P Fechine, *Solid State Phenomena* **202** (2013) 65.
30. H Serier-Brault, L Thibault, M Legrain, P Deniard, X Rocquefelte, P Leone, J-L Perillon, S Le Bris, J Waku, and S Jobic, *Inorg. Chem*. **53** (2014) 12378.
31. T Yoshimoto, T Goto, K Shimada, B Iwamoto, Y Nakamura, H Uchida, C A Ross, and M Inoue, *Adv. Elect. Mat*. **4** (2018) 1800106.
32. F W Aldbea, and N Ibrahim, *J. Mater. Sci. Appl.* **1** (2015) 185.
33. S Wemple, S Blank, J Seman, W Biolsi, *Phys. Rev. B* **9** (1974) 2134.
34. M H El Makdah, M H El-Dakdouki, R Mhanna, J Al Boukhari, and R Awad, *Appl. Phys. A* **127** (2021) 1.
35. M Kuila, U Deshpande, R Choudhary, P Rajput, D Phase, and V Raghavendra Reddy *J. Appl. Phys.* **129** (2021) 093903.
36. L Johnson, J Dillon Jr, J Remeika, *Phys. Rev. B* **1** (1970) 1935.
37. B Andlauer, J Schneider, and W Wettling, *Appl. Phys.* **10** (1976) 189.
38. H Liu, L Yuan, H Qi, S Wang, Y Du, Y Zhang, C Hou, and S Feng, *Dyes Pigm*. **145** (2017) 418.

39. D Wood and J Remeika, *J. Appl. Phys.* **38** (1967) 1038.
40. H Liu, H Qi, L Yuan, B Wang, C Hou, and S Feng, *Chem. Mater.* **31** (2019) 1048.
41. X Liu, A Staubitz, and T M Gesing, *ACS Appl. Mater. Interfaces* **11** (2019) 33147.
42. M Gaudon, P Deniard, L Voisin, G Lacombe, F Darnat, A Demourgues, J-L Perillon, and S Jobic, *Dyes Pigm.* **95** (2012) 344.
43. A Sawaby, M Selim, S Marzouk, M Mostafa, and A Hosny, *Physica B: Cond. Mater.* **405** (2010) 3412.
44. K Leon, D Mery, F Pedreschi, and J Leon, *Food Res. Int.* **39** (2006) 1084.
45. S L Levit, J Nguyen, N P Hattrup, B E Rabatin, R Stwodah, C L Vasey, M P Zeevi, M Gillard, P A D'Angelo, and K W Swana, *ACS Omega* **5** (2020) 7149.